Available online at www.sciencedirect.com
SCIENCE DIRECT
Cement and Concrete Research 36 (2006) 1023–1031
Cement and Concrete Research

X-ray photoelectron spectroscopic investigation of nanocrystalline calcium silicate hydrates synthesised by reactive milling

Leon Black [a,b,*], Krassimir Garbev [a], Günter Beuchle [a], Peter Stemmermann [a], Dieter Schild [c]

[a] Forschungszentrum Karlsruhe GmbH, Institut für Technische Chemie, Bereich Thermische Abfallbehandlung (ITC-TAB), Hermann-von-Helmholtz-Platz 1, 76344 Eggenstein-Leopoldshafen, Germany
[b] Materials and Engineering Research Institute, Sheffield Hallam University, Howard Street, Sheffield, S1 1WB, England, United Kingdom
[c] Forschungszentrum Karlsruhe GmbH, Institut für Nukleare Entsorgung (INE), Hermann-von-Helmholtz-Platz 1, 76344 Eggenstein-Leopoldshafen, Germany

Received 24 August 2005; accepted 22 March 2006

Abstract

X-ray photoelectron spectroscopy (XPS) has been used to analyse a series of mechanochemically synthesised, nanocrystalline calcium silicate hydrates (C-S-H). The samples, with Ca/Si ratios of 0.2 to 1.5, showed structural features of C-S-H(I). XPS analysis revealed changes in the extent of silicate polymerisation. Si 2p, Ca 2p and O 1s spectra showed that, unlike for the crystalline calcium silicate hydrate phases studied previously, there was no evidence of silicate sheets (Q^3) at low Ca/Si ratios. Si 2p and O 1s spectra indicated silicate depolymerisation, expressed by decreasing silicate chain length, with increasing C/S. In all spectra, peak narrowing was observed with increasing Ca/Si, indicating increased structural ordering. The rapid changes of the slope of FWHM of Si 2p, Δ_{Ca-Si} and Δ_{NBO-BO} as function of C/S ratio indicated a possible miscibility gap in the C-S-H-solid solution series between C/S 5/6 and 1. The modified Auger parameter (α') of nanocrystalline C-S-H decreased with increasing silicate polymerisation, a trend already observed studying crystalline C-S-H. Absolute values of α' were shifted about −0.7 eV with respect to crystalline phases of equal C/S ratio, due to reduced crystallinity.

Keywords: Calcium silicate hydrate (C-S-H); Characterization; Cement; XPS; Structure

1. Introduction

Poorly-crystalline calcium silicate hydrates (C-S-H gel) are the primary hydration products of Portland cements, and may constitute up to 70 wt.% of hardened cement pastes. Thus, the properties of these gels are important for the mechanical and chemical properties of cement based materials. C-S-H gels are commonly formed via the hydration of C_3S and β-C_2S, which are the principal constituents of Portland cement clinker. In hardened cement pastes, C-S-H gels are nanoheterogeneous, showing variable composition on a micrometric scale [1,2]. The C-S-H phases are often defined by their molar CaO/SiO_2 (C/S ratio). For C-S-H gel in fully reacted hydrated cement pastes it may vary over the range 1.7–2.0 (most probably 1.7–1.8) [2]. Ageing, carbonation, leaching, alkali–silica reaction (ASR), etc. meanwhile may cause the C/S ratio to drop well under 1.0.

In order to understand the structure of C-S-H phases and the processes of their formation, many investigations have been carried out on both hardened cement paste and synthetically produced C-S-H gels. The latter have the advantage of being able to be synthesised with a defined C/S ratio over a relatively broad range (0.5–1.5). Because of the possibility of intimate mixing of C-S-H gel with portlandite, some authors have suggested an actual upper limit of the C/S ratio of about 1.5 [3], whilst several authors investigated C-S-H phases for a possible miscibility gap, which may be present at around C/S = 1.0 [4].

The use of X-ray diffraction for structural investigations is a challenging task, due to the almost amorphous nature of the C-S-H gels. Nevertheless, they show some reflections in their diffraction patterns, which may be assigned mainly to ordering in the *xy* plane. A more ordered C-S-H phase of special importance is C-S-H(I), which also shows a basal reflection in the range 14–12Å and in most of its features resembles the pattern

* Corresponding author. Materials and Engineering Research Institute, Sheffield Hallam University, Howard Street, Sheffield, S1 1WB, England, United Kingdom. Tel.: +44 114 225 3062; fax: +44 114 225 3501.
E-mail address: l.black@shu.ac.uk (L. Black).

0008-8846/$ - see front matter © 2006 Elsevier Ltd. All rights reserved.
doi:10.1016/j.cemconres.2006.03.018

of tobermorite. The precise position of the basal reflection may depend upon C/S and water to solid, w/s, ratios [2]. Reactive milling in a ball mill is a reproducible way to synthesise nanocrystalline C-S-H phases of type C-S-H(I) which are the object of this investigation.

Because of the limitations of X-ray diffraction in the case of most C-S-H phases, structural studies have been performed with methods not dependent upon long-range structural order, such as trimethylsilylation (TMS) [5], ^{29}Si MAS NMR, [3,6–10] and vibrational spectroscopy [11,12]. Many structural models for C-S-H gel have been proposed based upon these investigations, mostly incorporating the binary solid solution mechanism. Results of both Fujii and Kondo [13] and Cong and Kirkpatrick [3] indicated that C-S-H gel exists as a solid solution between tobermorite and $Ca(OH)_2$, the so-called defect-tobermorite model, whilst Richardson and Groves [14] proposed a model based on isolated silicate chains of variable length and OH content, intergrown with $Ca(OH)_2$. A widely accepted model is that proposed by Taylor, assuming that C-S-H gel consists of a mixture of 14 Å tobermorite and jennite domains on the nanometer scale [15,16]. The structures of 14 Å tobermorite and jennite were solved recently by Bonacorssi et al. [17,18]. Richardson has recently stated that the precise structure of C-S-H depends upon the system in question, but may be adequately described by a combination of the tobermorite–jennite model and the tobermorite–portlandite model [19]. The applicability of these structure models seems to depend upon the nature and origin of the C-S-H gels. The models of Cong and Kirkpatrick suitably describe some synthetic C-S-H phases, whereas those of Taylor and Richardson and Groves address C-S-H gels obtained via hydration processes of cement. In both cases tobermorite-like structures similar to C-S-H(I) are very important for understanding the structural features of the C-S-H gel, despite limitations due to differences in the highest attainable C/S ratios depending upon the origin of the C-S-H gel.

In structural studies of C-S-H gels, the degree of polymerisation of the silicate units plays an essential role. ^{29}Si NMR investigations on pure C-S-H gels with various C/S ratios showed a decrease in the Q^1/Q^2 ratio and the occurrence of a Q^3 signal with decreasing C/S [3]. Vibrational spectroscopy studies [11,12] also confirm these observations. Increased polymerisation has also been observed after heating of pure C-S-H gels [20] or leaching of hardened cement pastes [21].

Okada et al. [22] studied the silicate anionic structure of the C-S-H phases formed upon hydration of β-C_2S, by means of TMS and ^{29}Si NMR spectroscopy. They reported increasing polymerisation, from monomer to dimer then chain-polymer, with increasing curing time. Similar observations were made by Rodger et al. [23] for C_3S. Grutzeck et al. [24,25] and Rodger et al. [23] showed that cement pastes are comprised initially of dimers (Q^1), which transform to Q^2 upon ageing. Thomas et al. [26] showed that a further polymerisation to Q^3 and Q^4 of the C-S-H gels is possible in mature and partly carbonated cement pastes.

Here, following a cursory analysis by X-ray diffraction, we have studied a series of synthetically prepared C-S-H phases of type C-S-H(I) using X-ray photoelectron spectroscopy (XPS), a technique more thoroughly reviewed elsewhere [27,28]. This technique is extremely surface sensitive, and has therefore, been used to examine the early stages of hydration [29–32]. It is possible, using XPS, to investigate the chemical state of all elements, excluding hydrogen, in a single experiment, giving a total analysis time per sample of about 1 to 2 h. Slight changes in the bonding environment of a given element results in changes in photoelectron spectra. Thus, with emphasis on studies of C-S-H phases, photoelectron spectra are sensitive, for example, to the degree of polymerisation of the silicate anionic structure [31,33–36], to the calcium coordination number [33], to the bonding state of oxygen (i.e. the presence of bridging and non-bridging oxygen atoms) [30,33,37], and to the influence of atomic substitution [38]. Furthermore, XPS is quantitative, allowing the effects of C/S upon structure to be readily discerned. For these reasons, XPS is suitable for structural examinations of C-S-H gels. Many of the studies using XPS for the analysis of cements have concentrated upon the quantitative capabilities of the technique, i.e. determination of C/S ratios, rather than for structural analysis, i.e. determination of silicate structure. Upon hydration of C_3S [29–31] and β-C_2S [32], changes in photoelectron spectra were observed, indicating changes in bonding structure, but not commented upon. Mollah et al. [36] did however note increased Si 2p binding energies upon hydration of Portland cement clinker phases attributed to increased silicate polymerisation.

We have recently shown how XPS may be used to ascertain structural information from C-S-H phases. Increased silicate polymerisation, as a result of decreasing C/S, led to an increase in the silicon binding energies of a series of crystalline C-S-H phases [33,34,38]. Similarly, ageing of fresh clinker minerals led to surface hydration and silicate polymerisation, observed via marked increases in silicon binding energies [37]. Calcium binding energies have also been found to be dependent upon C-S-H structure, with six-fold coordinated calcium, as present in C-S-H phases with sheet structures, typically possessing higher binding energies than C-S-H phases with either chain or dimeric silicate structures [33]. Furthermore, the O 1s spectra of the crystalline C-S-H phases may also be used to reveal structural changes, in particular the preponderance of bridging and non-bridging oxygen atoms in the structures [33,35].

This article is a continuation of recent studies, progressing from crystalline analogues to laboratory-synthesised, pure, homogeneous, mechanochemically-synthesised calcium silicate hydrates. An initial cursory analysis by X-ray diffraction was used to confirm structure. X-ray photoelectron spectroscopy (XPS) was then used to investigate changes in structure with changes in C/S. Whilst the samples analysed in this study were synthetic, and may therefore not entirely model the C-S-H phases formed in hydrated cement pastes, it is hoped that this work will act as a step towards the use of XPS to analyse hydrated cement pastes.

2. Experimental

2.1. Synthesis

The nanocrystalline C-S-H phases were prepared mechanochemically, according to the method of Saito et al. [39] from stoichiometric mixtures of CaO (freshly prepared from $CaCO_3$ at 1000 °C for 5 h) and SiO_2 (Aerosil). This entailed milling of

the oxides with distilled water (w/s = 8) in an agate ball mill for 24 h. After every 20 min of milling, the ball mill was stopped for 10 min to avoid overheating. All syntheses were performed under nitrogen atmospheres to minimise the effects of carbonation. After milling, the slurries produced were dried in a glovebox, under nitrogen, at 60 °C for 96 h. The following samples with target C/S-ratios were synthesised: C/S = 1/5, 2/5, 1/2, 2/3, 3/4, 5/6, 1/1, 4/3 and 3/2. In the following discussion the samples will be referred to using this notation. After synthesis, and between analyses, the samples were stored under nitrogen in hermetically-closed glass vials.

2.2. XPS

The powdered samples were smoothly pressed, as received, onto indium foil and introduced into the spectrometer for analysis. XPS spectra were recorded on a PHI 5600 spectrometer (7×10^{-8} Pa base pressure), fitted with a Mg Kα anode (1253.6 eV). High resolution scans of elemental lines were collected at 11.75 eV pass energy of the hemispherical capacitor analyser which yields a full-width-at-half-maximum (FWHM) of the Ag $3d_{5/2}$ line of 0.62 eV. The energy scale of the spectrometer was calibrated using the Cu $2p_{3/2}$, Ag $3d_{5/2}$, and Au $4f_{7/2}$ lines of pure and Ar^+ sputter cleaned metal foils [40]. The binding energies of elemental lines were charge referenced to the C 1s line of adventitious hydrocarbon at a binding energy (BE) of 284.8 eV. The error in the binding energies is about ±0.15 eV and for the FWHM about ±0.05 eV, assuming similar charging situations at the sample surfaces.

High resolution spectra were recorded from the Si 2p, Ca 2p, O 1s and C 1s regions. Data were analysed using PHI Multipak software. Curve fitting was performed using nonlinear-least-squares optimization of Gaussian–Lorentzian sum functions. A Shirley-type background was used for all background subtraction corrections. Atomic concentrations were calculated with regard to transmission function of the spectrometer and standard sensitivity factors. Note that the Si 2p spectra were fitted using one curve, rather than the two predicted by XPS theory. This allows a more ready comparison with literature values and avoids the confusion encountered previously [33,34].

3. Results and discussion

Pure C-S-H was obtained in the samples with C/S ~ 1/2 to 1. X-ray diffraction patterns were typical for nanocrystalline C-S-H (C-S-H (I)), and may be identified according to ICDD data set entry No. 34-0002 (Fig. 1). Furthermore, there was no similarity between the diffraction patterns of our samples and the C-S-H (II) phase (ICDD data set entry No. 27-0374). With increasing C/S the basal reflection shifted to lower d-spacings, with a simultaneous decrease in FWHM. XRD analysis of the samples is the subject of a separate paper [41]. At higher calcium contents (C/S 4/3, 3/2) additional peaks were visible, ascribed to portlandite, the quantity of which increased with increasing C/S. At lower calcium contents (C/S 1/5, 2/5) a hump at ~4 Å was observed, attributed to amorphous silica gel. No reflections of any $CaCO_3$ polymorphs were visible in the diffraction patterns. Some surface carbonation is inevitable during analysis, but the quantity of carbonate produced lay under the detection limits of the technique.

Quantification of the photoelectron spectra showed a good correlation between as-weighed and measured C/S ratios (as determined from peak intensities and empirical sensitivity factors), indicating no significant surface enrichment of either calcium or silicon for the samples. This allowed surface composition

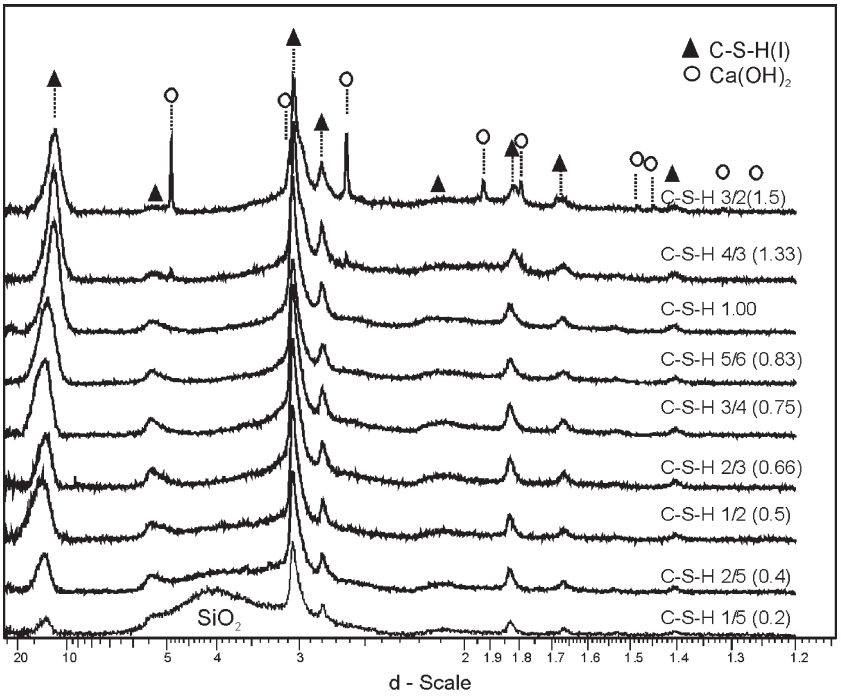

Fig. 1. XRD powder patterns of the nanocrystalline C-S-H phases with different C/S ratios (device: D8 Advance, Cu $K\alpha_{1,2}$).

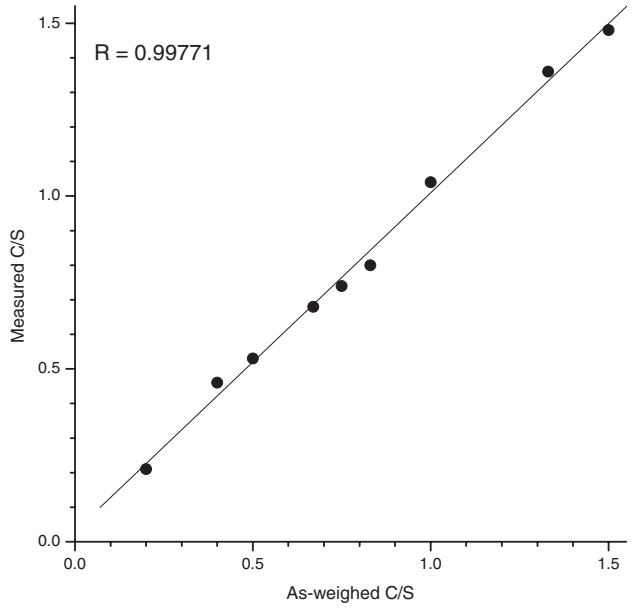

Fig. 2. Plot of measured (by XPS) against as-weighed C/S ratios of the nanocrystalline C-S-H samples.

to be used in place of bulk composition for most of the samples (see below). Fig. 2 plots the measured C/S ratios against the intended C/S ratios.

Fig. 3 shows a plot of Si 2p binding energies and peak widths versus measured C/S ratios. The binding energies lay between 101.65 and 102.9 eV. However, the samples with C/S = 1/5 and 2/5 were not homogeneous with respect to silicon-bearing phases, and contained amorphous silica as visible in the X-ray diffraction patterns (see above). This has also been determined by Raman spectroscopy [42] and ^{29}Si NMR [43]. Excluding these samples, the range in Si 2p binding energies was smaller, i.e. 102.2 to 101.65 eV. These binding energies are similar to those reported for hardened cement pastes [36] and aged cement clinkers [35]. There was a slight decrease in Si 2p binding energies with increasing C/S, indicating silicate depolymerisation, as observed for crystalline silicates [33,34,44,45]. The binding energies for various crystalline C-S-H phases are also given in Fig. 3 for comparison. The Si 2p binding energies of the nanocrystalline samples were similar to those of the crystalline neso-, soro-, and inosilicates (Q^0, Q^1 and Q^2 silicates respectively) [33,34] whilst being considerably lower than those of crystalline phyllosilicates (Q^3 silicates). It follows that nanocrystalline C-S-H phases do not form sheet silicate structures. Rather, they comprise silicate dimers and chains, as has also been confirmed by Raman spectroscopy [42] and ^{29}Si NMR [43]. It is also consistent with the ^{29}Si NMR spectroscopic data of Cong and Kirkpatrick [3], who observed a small quantity of Q^3 bonding environments in samples with C/S < 5/6. These were assigned to bridging tetrahedra between two single chains giving rise to double chains as found in xonotlite and 11 Å tobermorite, rather than to sheet structures. Okada et al. [46] observed only long chains and no silicate sheets in C-S-H gels with C/S ratios of 1/2 and 2/3.

Fig. 3 also shows the variation in peak width (FWHM) of the nanocrystalline samples with C/S. As expected, the heterogeneous, silicon-rich samples (C/S = 1/5 and 2/5), which contain amorphous silica, with a characteristic binding energy of ~103.4 eV [47], gave rise to broad peaks. More interestingly there was a marked increase in peak width from C/S 5/6 to 1/2. If we consider that variations in binding energies reflect differences in the electronic environment of an element, then sharper peaks indicate the presence of fewer environments, i.e. a more ordered structure. Thus, we may assume that the polymerisation at lower C/S ratios (C/S 2/5–1/2) is not uniform, rather that there is a mixture of different silicate arrangements, namely Q^3, Q^2 dimers and Q^2 chain ends. Based upon the diffraction patterns shown earlier, some broadening of the Si 2p

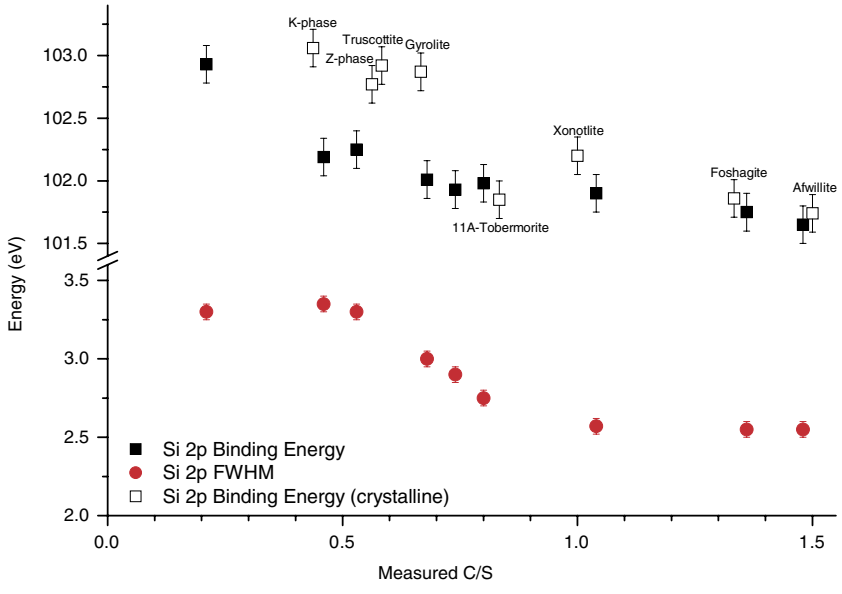

Fig. 3. Si 2p binding energies and peak widths versus C/S for the various nanocrystalline C-S-H phases. Also shown, for comparison, are the Si 2p binding energies of various crystalline C-S-H phases.

peak may be due to the presence of amorphous silica, but the resolution was insufficient to identify separate phases within the samples of low C/S. Additionally, the change in slope of FWHM in Fig. 3 may indicate a possible miscibility gap in the C-S-H solid solution series between C/S 5/6 and 1. Finally, we consider the samples with C/S = 4/3 and 3/2. These samples contained considerable amounts of portlandite. A detailed interpretation of the diffraction patterns revealed that the C-S-H phases in these samples both have C/S ratios of ~1.25 [41], with the excess calcium present as portlandite. On the basis of Si 2p photoelectron spectra alone it would not be possible to ascertain this, but with the knowledge obtained from XRD we see that the Si 2p binding energies of these two calcium-rich samples are similar, as are their FWHM. From this we may infer that the silicon-bearing phases in these samples, i.e. C-S-H, are similar.

The modified Auger parameter α' (defined as the sum of the Si 2p photoelectron binding energy and the SiKLL Auger electron kinetic energy) is frequently used as a measure of extra-atomic relaxation and can be employed as a probe of the local structural of the element under investigation. For crystalline C-S-H phases, α' has successfully been used to characterise the polymerisation of silicate tetrahedra [33–35]. For the crystalline C-S-H phases, α' decreases with increased polymerisation, which may be interpreted as follows. The extra-atomic relaxation of final state silicon depends on screening by electrons of neighbouring atoms. In silicates, these nearest neighbours are, to a first approximation, oxygen atoms. Screening is increasingly effective, as more electrons around a specific oxygen atom are polarised towards the silicon atom. In other words, the lower the electronegativity of additional cations bonded to the oxygen, the better the screening effect. Bridging oxygen atoms are bonded to a second silicon atom and thus reduce screening of the central silicon. Non-bridging oxygen atoms are bound to calcium atoms, which, being less electronegative than silicon lead to increased shielding of the silicon. Increased polymerisation leads to a greater number of bridging oxygen atoms, therefore decreased shielding and lower α'.

The modified Auger parameters of the nanocrystalline C-S-H phases followed the trend observed for the crystalline phases, and decreased with increasing polymerisation (Fig. 4) (using the mean connectivity as a simple measure of polymerisation [48]). Mean connectivity was calculated based on ^{29}Si NMR data [43] (note that no NMR data were obtained for the sample with C/S = 1/5). It is also possible to see clustering of the samples, with the two sets of bi-phase samples, i.e. at the extremities of C/S, separated from the monophase samples with $1/2 < C/S < 1/1$. Absolute values of α' were consistently shifted by about −0.7 eV with respect to the crystalline phases of equal C/S ratio. Considering the data for the three silica polymorphs, it is clear that α' increases with increasing crystallinity. Thus, the lower crystallinity of the nanocrystalline samples compared to their crystalline equivalents leads to this reduction in α'.

Whilst well-defined trends were visible in the Si 2p binding energies and especially in the Auger parameters, the Ca $2p_{3/2}$ binding energies showed no such behaviour (Fig. 5). Nanocrystalline C-S-H phases in general possessed Ca $2p_{3/2}$ binding energies of 346.9 ± 0.15 eV, similar to crystalline neso-, soro-, and inosilicates. The crystalline phyllosilicates (sheet silicates) have slightly higher binding energies (>347.25 eV) [33]. This may be taken as further evidence for the absence of silicate sheets in our phases. The Ca $2p_{3/2}$ peaks sharpened with increasing C/S, again implying a more ordered structure with

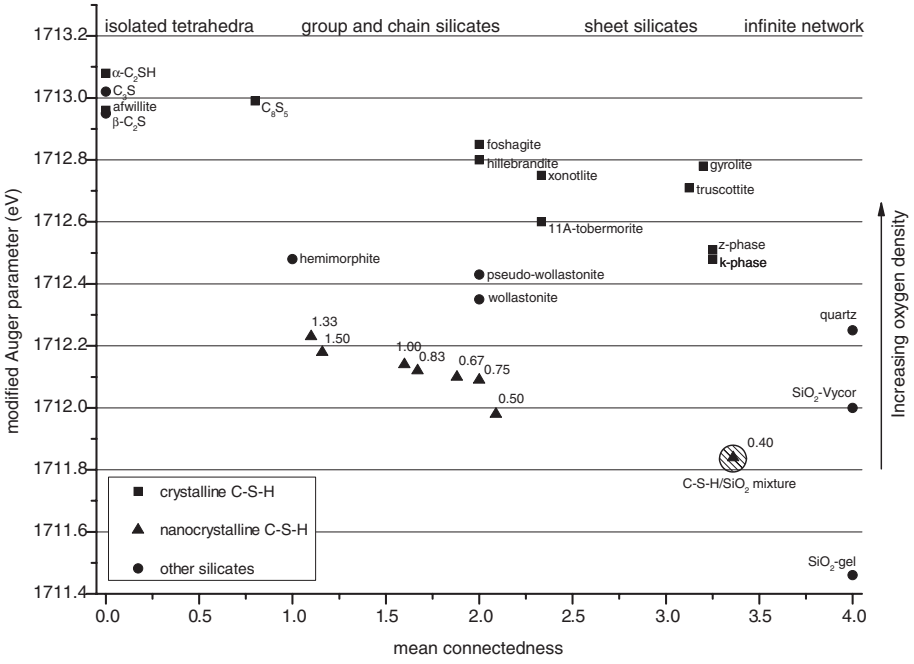

Fig. 4. Modified-Auger-parameter plotted against mean connectivity of pure crystalline and nanocrystalline C-S-H phases (Note that the annotations for the nanocrystalline C-S-H phases indicates the as-weighed C/S ratio). Modifications of silica and some other calcium silicates are given for comparison. Mean connectivity of pure nanocrystalline samples was obtained from ^{29}Si NMR measurements.

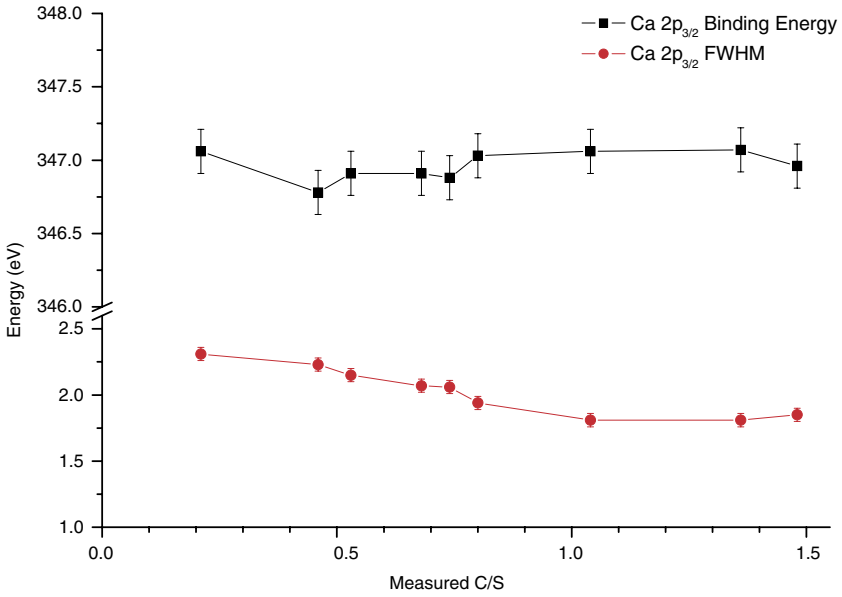

Fig. 5. Ca $2p_{3/2}$ binding energies and peak widths versus C/S for the various nanocrystalline C-S-H phases. Note, the axes are plotted on the same scale as Fig. 3 for ready comparison.

increasing C/S. As with the Si 2p spectra, it wasn't possible to identify a second phase within the calcium-rich samples, despite portlandite being detected by XRD.

The energy separation between the Ca $2p_{3/2}$ and Si 2p peaks, (Δ_{Ca-Si}), has previously been used to follow silicate polymerisation upon hydration of C_3S [29] and C_2S [32], there being a decrease in energy separation upon hydration, i.e. silicate polymerisation. This approach has the advantage of negating errors due to charge correction, but does not allow comparisons between phases that are too dissimilar.

Fig. 6 plots Δ_{Ca-Si} versus C/S for the nanocrystalline phases. The separation increased from ~244.6 eV for the sample with C/S=2/5 (ignoring the highly heterogeneous sample with C/S=1/5), to ~245.3 eV for the samples with C/S=4/3 and 3/2. This is further proof for increased silicate polymerisation with decreasing C/S. For comparison, Regourd et al. observed an energy separation of 245.7 eV for C_3S, falling to 245.1 eV after 4 h hydration [29]. A similar study by Thomassin et al. observed an initial energy separation of 245.4 eV for β-C_2S, falling to 244.6 eV after 4 h hydration [32]. We have reported similar results for fresh and aged clinker minerals [35]. Calculations based on the results of Mollah et al. show that, upon curing of OPC for 28 days, the energy separation decreased from 246.3 to 244.8 eV and 245.9 eV for pure and zinc-doped OPC respectively [36].

Interestingly, although the samples with C/S=4/3 and 3/2 ostensibly had different C/S ratios, Δ_{Ca-Si} values indicated phases of similar structure. The XRD patterns of these two samples were

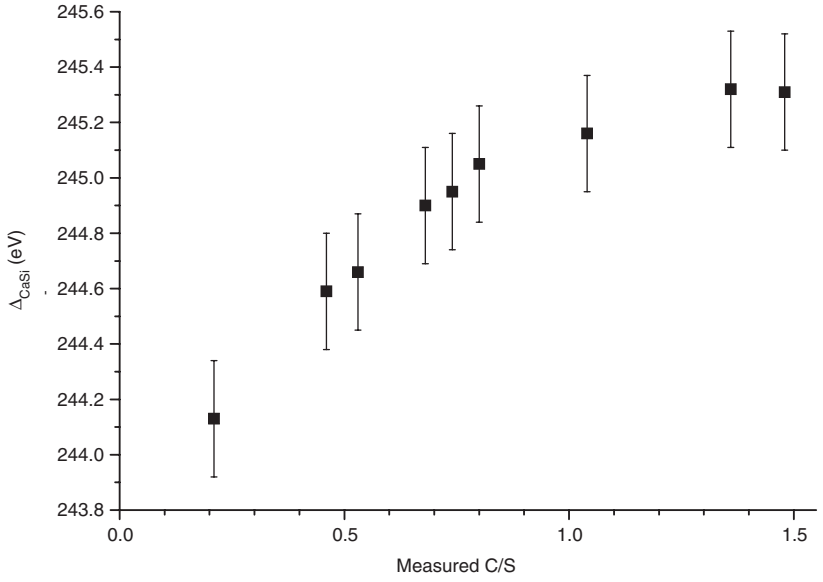

Fig. 6. Energy separation between Si 2p and Ca $2p_{3/2}$ binding energies (Δ_{Ca-Si}) versus C/S for the various nanocrystalline C-S-H phases.

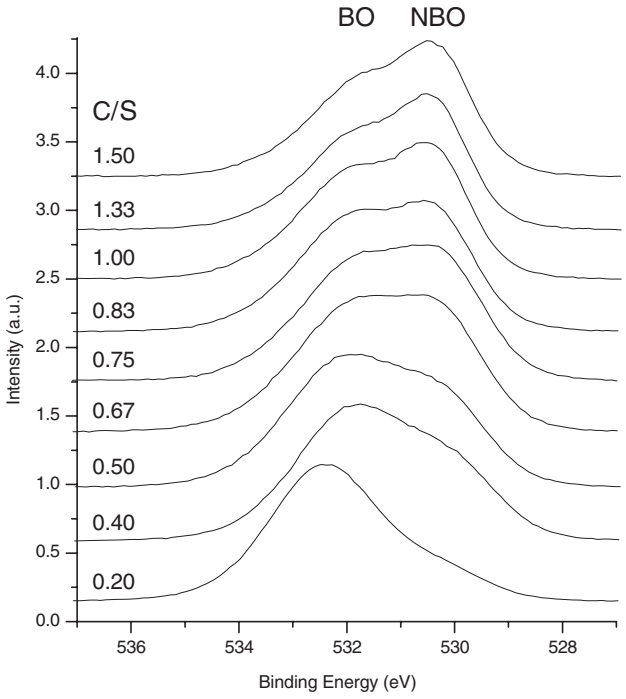

Fig. 7. O 1s spectra of the nanocrystalline C-S-H phases, showing the variation, with C/S, in the relative numbers of bridging (BO) and non-bridging oxygen (NBO) atoms. Spectral intensities have been normalised for comparison.

very similar except for the portlandite contents, and the C-S-H phases both had C/S ratios of ~1.25 (see above) [41].

Finally, we consider the O 1s spectra, which may be employed to examine the structure of minerals [44,45,49] and glasses [50–52], for example to distinguish bridging oxygen (BO) and non-bridging oxygen (NBO) atoms. The binding energy of an element is directly related to its effective atomic charge. Increased electron density around an atom screens the core electrons, leading to a decreased binding energy. Therefore, non-bridging oxygen atoms, especially when bound to alkali and alkali earth metals, often have lower binding energies than bridging oxygen atoms. We have recently shown how the O 1s spectra of crystalline C-S-H phases could be related to their structures [37].

Fig. 7 shows the O 1s spectra of the nanocrystalline phases. The spectra may be assumed to comprise of four components: non-bridging oxygen atoms with binding energies of 530–530.5 eV, bridging oxygen atoms with binding energies of 531.5–532.7 eV, hydroxide species at 533–533.5 eV and bound water at ~534 eV. With respect to the minor phases present at both ends of the investigated composition range, amorphous silica, containing bridging oxygen atoms, does not add additional components. Portlandite in the calcium-rich samples adds intensity at 531.6 eV [53]. For the nanocrystalline C-S-H phases, signals were visible from bridging, non-bridging and hydroxyl species, with little or no contribution from bound water. The high vacuum conditions required for XPS analysis lead inevitably to some loss of bound water [37,54]. However, loss of such water should not influence the extent of silicate polymerisation, nor the contributions from either bridging or non-bridging oxygen atoms.

The O 1s spectra were broad and asymmetric. With increasing C/S there were increased contributions from non-bridging oxygen atoms, as silicate depolymerisation led to increased numbers of Ca–O–Si units and fewer Si–O–Si units. However, the Si 2p spectra showed that silicate sheets are not formed. Thus, the observed silicate depolymerisation was due to ever shortening silicate chains with increasing C/S.

For crystalline phases, BO/NBO ratios have been successfully linked to crystal structure, with an increase in the BO/NBO ratio being linked to increased silicate polymerisation [37]. Despite the structures of the crystalline C-S-H phases already being known, the extraction of data was an arduous task. Fitting parameters had to be strenuously constrained, and loosened

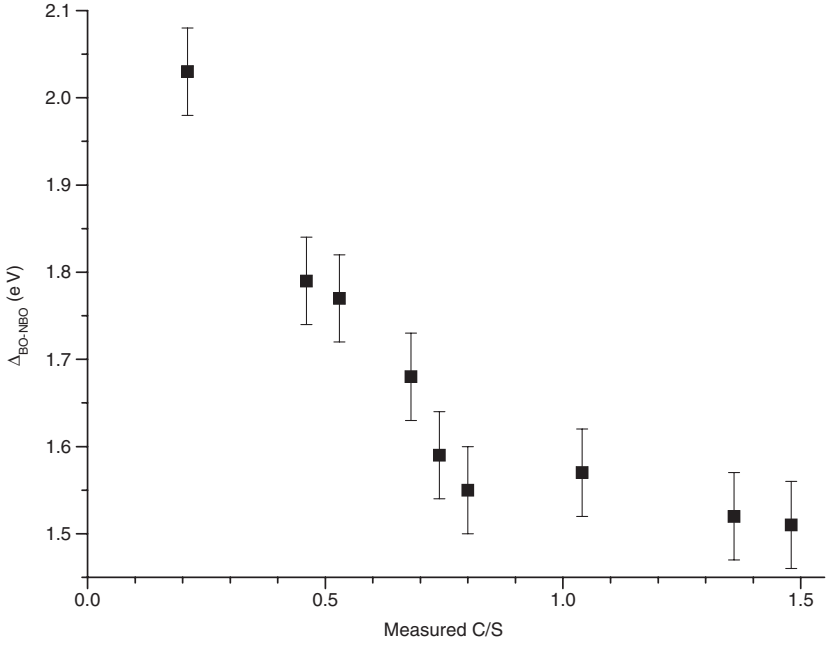

Fig. 8. Variation in Δ_{NBO-BO} with C/S. The decrease in peak separation corresponds to increased silicate polymerisation.

gradually with each iteration to ensure sensible results. The lack of a structural model for the nanocrystalline C-S-H phases, from which to begin peak fitting made structural interpretations based on BO/NBO ratios incredibly difficult. The problems were compounded by the presence of minor phases, namely unreacted silica and portlandite. Unlike with the Si 2p and Ca 2p spectra, the presence of these minor phases could be observed directly in the O 1s spectra. The presence of a large excess of unreacted SiO_2 in the sample with C/S = 1/5 was clearly evident in this sample's O 1s spectrum, there being a large peak at ~532.5 eV. This peak was not evident however in the sample with C/S = 2/5, where XRD also showed the presence of unreacted SiO_2. More subtle were the changes in the spectra of the calcium-rich samples. The O 1s binding energy of portlandite is close to that of bridging oxygen atoms. The O 1s spectra of the samples with C/S = 4/3 and 3/2 revealed little difference compared to the sample with C/S = 1/1, where an increase in the NBO/BO ratio was expected. The overlapping O 1s bands due to portlandite and bridging oxygen atoms gave a lower than expected NBO/BO ratio.

Changes in the extent of polymerisation can also be followed via changes in the separation between the peaks due to bridging and non-bridging oxygen atoms (Δ_{NBO-BO}) [37]. Fig. 8 shows a continuously increasing peak separation with decreasing C/S. We recently observed similar behaviour in crystalline C-S-H phases with sheet and chain silicate structure, where peak separation increased with decreasing C/S within each structural class [37]. The shift from chain to sheet silicate structures was on the other hand marked by a strong discontinuity in peak separation. Hence, like the crystalline phases, the nanocrystalline C-S-H phases are increasingly polymerised with decreasing C/S ratio. Unlike the crystalline phases however, increased polymerisation manifests itself in the formation ever lengthening silicate chains rather than sheet silicate structures. Absolute values of peak separation were higher for nanocrystalline C-S-H, indicating a maximum NBO/Ca ratio of 2, particularly for C/S ~ 1/2 [37]. Again with regard to a possible miscibility gap in the C-S-H-solid solution series, there seems to be a change in slope around C/S 0.9.

4. Conclusions

Nanocrystalline calcium silicate hydrate (C-S-H) samples were prepared mechanochemically in the composition range with C/S ratios of 1/5–3/2, yielding surface C/S ratios, as confirmed by XPS measurement, of between 0.21 and 1.48. The samples with C/S = 1/5 and 2/5 were found to contain residual SiO_2, and samples with C/S 4/3 and 3/2 contained portlandite. The C-S-H gave diffraction patterns similar to C-S-H(I). The phases appeared to possess a defect-tobermorite structure, as indicated by the results of Cong and Kirkpatrick [3], because no C-S-H(II) or other phase similar to jennite could be found. This structure is consistent for synthetic C-S-H phases.

Quantitative XPS showed the average surface composition to match the bulk composition. However, where XRD revealed multiphase systems for the most calcium-rich or calcium-poor samples, XPS could not easily recognise the presence of multiple phases. Despite this, the surface structure may be used to investigate bulk structure. This is true for the monophase samples (1/2 < C/S < 1/1), and for the multiphase systems, provided that the XPS data are used in conjunction with other techniques, i.e. XRD, Raman or NMR.

XPS enabled the simultaneous determination of the chemical states of all of the constituent elements (excluding hydrogen). Si 2p binding energies slightly decreased with increasing C/S. The binding energies indicated the presence of neso-, soro- or inosilicates, not phyllosilicates (sheet silicates). Further evidence for this was gained from examining variations in Ca 2p binding energies, where the higher Ca 2p binding energies seen for phyllosilicates were not observed for the nanocrystaline C-S-H phases.

The trend in modified Auger parameter for the nanocrystalline C-S-H followed that seen for crystalline C-S-H, with a decrease in α' with increasing C/S indicating decreased polymerisation. Absolute values of α' were shifted about −0.7 eV with respect to crystalline phases of equal C/S ratio, due to a lower degree of crystallinity.

The O 1s spectra also indicated silicate depolymerisation with increasing C/S. As the presence of silicate sheets was excluded, silicate depolymerisation indicated decreasing silicate chain length with increasing C/S. At low C/S, the presence of unreacted SiO_2 was observed in the O 1s spectra, whilst at high C/S the presence of portlandite led to erroneous NBO/BO ratios.

All spectra (Si 2p, Ca 2p and O 1s) also showed consistent behaviour when examining changes in peak widths with C/S. Peak widths were greatest for the calcium-poor phases and fell consistently with increasing C/S. From this we may infer that there was greater structural disorder within the calcium-poor phases.

There were several hints on a possible miscibility gap in the C-S-H-solid solution series between C/S 5/6 and 1. The slope of FWHM of Si 2p versus C/S changed rapidly in this region, as did the appearance of the O 1s spectra, and Δ_{NBO-BO} versus C/S.

References

[1] I.G. Richardson, Cem. Concr. Res. 29 (1999) 1131–1147.
[2] H.F.W. Taylor, Cement Chemistry, 1st edn., Academic Press, 1990, pp. 123–166.
[3] X.D. Cong, R.J. Kirkpatrick, Adv. Cem. Based Mater. 3 (3/4) (1996) 144–156.
[4] H. Viallis-Terrisse, A. Nonat, J. Colloid Interface Sci. 244 (1) (2001) 58–65.
[5] L.S. Dent-Glasser, E.E. Lachowski, K. Mohan, H.F.W. Taylor, Cem. Concr. Res. 8 (1978) 733–739.
[6] E. Lippmaa, M. Magi, M. Tarmak, W. Wieker, A.-R. Grimmer, Cem. Concr. Res. 12 (1982) 597–602.
[7] I.G. Richardson, A.R. Brough, R. Brydson, G.W. Groves, C.M. Dobson, J. Am. Ceram. Soc. 76 (2000) 2285–2288.
[8] I.G. Richardson, A.R. Brough, G.W. Groves, C.M. Dobson, Cem. Concr. Res. 24 (1994) 813–829.
[9] X.D. Cong, R.J. Kirkpatrick, S. Diamond, Cem. Concr. Res. 23 (1993) 811–823.
[10] P. Colombet, A.-R. Grimmer (Eds.), Nuclear Magnetic Resonance Spectroscopy of Cement Based Materials, Springer Verlag, Heidelberg, 1998.
[11] R.J. Kirkpatrick, J.L. Yarger, P.F. McMillan, P. Yu, X.D. Cong, Adv. Cem. Based Mater. 5 (1997) 93–99.

[12] P. Yu, R.J. Kirkpatrick, B. Poe, P.F. McMillan, X. Cong, J. Am. Ceram. Soc. 82 (3) (1999) 724–748.
[13] K. Fujii, W. Kondo, J. Am. Ceram. Soc. 66 (12) (1983) 220–221.
[14] I.G. Richardson, G.W. Groves, J. Mater. Sci. 27 (1992) 6204–6212.
[15] H.F.W. Taylor, J. Am. Ceram. Soc. 69 (1986) 464–467.
[16] H.F.W. Taylor, Z. Kristallogr. 202 (1992) 41–50.
[17] E. Bonaccorsi, S. Merlino, H.F.W. Taylor, Cem. Concr. Res. 34 (2004) 1481–1488.
[18] E. Bonaccorsi, S. Merlino, A.R. Kampf, J. Am. Ceram. Soc. 88 (3) (2005) 505–512.
[19] I.G. Richardson, Cem. Concr. Res. 34 (9) (2004) 1733–1777.
[20] X. Cong, R.J. Kirkpatrick, Cem. Concr. Res. 25 (6) (1995) 1237–1245.
[21] J.D. Ortego, Y. Barroeta, F.K. Cartledge, H. Akhter, Environ. Sci. Technol. 25 (1991) 1171–1174.
[22] Y. Okada, H. Ishida, K. Sasaki, J.F. Young, T. Mitsuda, J. Am. Ceram. Soc. 76 (5) (1994) 1313–1318.
[23] S.A. Rodger, G.W. Groves, N.J. Clayden, C.M. Dobson, in: L.J. Struble, P.W. Brown (Eds.), Microstructural Developments during Hydration of Cement, Mat. Res. Soc. Symp. Proc., vol. 85, Materials Research Society, Pittsburgh, PA, 1987, pp. 13–20.
[24] M. Grutzeck, A. Benesi, B. Fanning, J. Am. Ceram. Soc. 72 (1989) 665–668.
[25] M.W. Grutzeck, S. Kwan, J.L. Thompson, A. Benesi, J. Mater. Sci. Lett. 18 (1999) 217–220.
[26] S. Thomas, K. Meise-Gresch, W. Müller-Warmuth, I. Odler, J. Am. Ceram. Soc. 76 (8) (1993) 1998–2004.
[27] D. Briggs, M.P. Seah, Practical Surface Analysis Vol 1 — Auger and X-ray Photoelectron Spectroscopy, 2nd edn.,Wiley, Chichester, UK, 1994.
[28] M.F. Hochella Jr., in: F.C. Hawthorne (Ed.), Reviews in Mineralogy Vol 18 — Spectroscopic Methods in Mineralogy and Geology, Mineralogical Society of America, Washington DC, 1988, pp. 573–637.
[29] M. Regourd, J.H. Thomassin, P. Baillif, J.C. Touray, Cem. Concr. Res. 10 (1980) 223–230.
[30] D. Ménétrier, I. Jawed, T.S. Sun, J. Skalny, Cem. Concr. Res. 9 (1979) 473–482.
[31] S. Long, C. Liu, Y. Wu, Cem. Concr. Res. 28 (2) (1998) 245–249.
[32] J.H. Thomassin, M. Regourd, P. Baillif, J.C. Touray, C. R. Acad. Sci. C Chim. 290 (Jan 1980) 1–3.
[33] L. Black, K. Garbev, P. Stemmermann, K.R. Hallam, G.C. Allen, Cem. Concr. Res. 33 (6) (2003) 899–911.
[34] L. Black, K. Garbev, P. Stemmermann, K.R. Hallam, G.C. Allen, Cem. Concr. Res. 33 (11) (2003) 1913.
[35] L. Black, A. Stumm, K. Garbev, P. Stemmermann, K.R. Hallam, G.C. Allen, Cem. Concr. Res. 33 (10) (2003) 1561–1565.
[36] M.Y.A. Mollah, T.R. Hess, Y.-N. Tsai, D.L. Cocke, Cem. Concr. Res. 3 (1993) 773–784.
[37] L. Black, K. Garbev, P. Stemmermann, K.R. Hallam, G.C. Allen, Phys. Chem. Miner. 31 (6) (2004) 337–346.
[38] L. Black, A. Stumm, K. Garbev, P. Stemmermann, K.R. Hallam, G.C. Allen, Cem. Concr. Res. 35 (2005) 51–55.
[39] F. Saito, G. Mi, M. Hanada, Solid State Ion. 101–103 (1997) 37–43.
[40] M.P. Seah, I.S. Gilmore, G. Beamson, Surf. Interface Anal. 26 (1998) 642–649.
[41] K. Garbev, G. Beuchle, L. Black, M. Bornefeld, P. Stemmermann, in preparation.
[42] L. Black, C. Breen, K. Garbev, P. Stemmermann, Abstracts of the Cement and Concrete Science Conference, 16–17th September 2004, University of Warwick, 2004.
[43] G. Beuchle, pers comm.
[44] H. Seyama, M. Soma, J. Chem. Soc., Faraday Trans. 81 (1985) 485–495.
[45] K. Okada, Y. Kameshima, A. Yasumori, J. Am. Ceram. Soc. 81 (7) (1998) 1970–1972.
[46] Y. Okada, T. Masuda, H. Ishida, Nippon Seramikkusu Kyokai Gakujutsu Ronbunshi — J. Ceram. Soc. Jpn. 103 (2) (1995) 124–127.
[47] C.D. Wagner, D.E. Passoja, H.F. Hillery, T.G. Kinisky, H.A. Six, W.T. Jansen, J.A. Taylor, J. Vac. Sci. Technol. 21 (4) (1982) 933–944.
[48] F. Liebau, Structural Chemistry of Silicates, Springer Verlag, Heidelberg, 1985.
[49] H. Seyama, M. Soma, A. Tanaka, Chem. Geol. 129 (1996) 209–216.
[50] D.S. Goldman, Phys. Chem. Glasses 27 (3) (1986) 128–133.
[51] C. Schultz-Münzenberg, W. Meisel, P. Gütlich, J. Non-Cryst. Solids 238 (1998) 83–90.
[52] A. Mekki, M. Salim, J. Electron Spectrosc. 101–103 (1999) 227–232.
[53] NIST Standard Reference Database 20, Version 3.4 (Web Version), Data compiled and evaluated by Charles D. Wagner, Alexander V. Naumkin, Anna Kraut-Vass, Juanita W. Allison, Cedric J. Powell, and John R. Rumble, Jr. Release date: August, 2003.
[54] R.N.J. Comans, T.T. Eighmy, E.L. Shaw, Surf. Sci. Spectra 4 (2) (1996) 150–156.